

Article

Pharmacokinetics and disposition of anlotinib, an oral tyrosine kinase inhibitor, in experimental animal species

Chen-chun ZHONG^{1,2}, Feng CHEN¹, Jun-ling YANG¹, Wei-wei JIA¹, Li LI¹, Chen CHENG¹, Fei-fei DU¹, Su-ping ZHANG¹, Cheng-ying XIE¹, Na-ting ZHANG¹, Olajide E OLALAYE¹, Feng-qing WANG¹, Fang XU¹, Li-guang LOU¹, Dong-ying CHEN¹, Wei NIU^{1,*}, Chuan LI^{1,2,*}

¹State Key Laboratory of Drug Research, Shanghai Institute of Materia Medica, Chinese Academy of Sciences, Shanghai 201203, China; ²University of Chinese Academy of Sciences, Shanghai 201203, China

Abstract

Anlotinib is a new oral tyrosine kinase inhibitor; this study was designed to characterize its pharmacokinetics and disposition. Anlotinib was evaluated in rats, tumor-bearing mice, and dogs and also assessed *in vitro* to characterize its pharmacokinetics and disposition and drug interaction potential. Samples were analyzed by liquid chromatography/mass spectrometry. Anlotinib, having good membrane permeability, was rapidly absorbed with oral bioavailability of 28%–58% in rats and 41%–77% in dogs. Terminal half-life of anlotinib in dogs (22.8±11.0 h) was longer than that in rats (5.1±1.6 h). This difference appeared to be mainly associated with an interspecies difference in total plasma clearance (rats, 5.35±1.31 L·h⁻¹·kg⁻¹; dogs, 0.40±0.06 L·h⁻¹·kg⁻¹). Cytochrome P450-mediated metabolism was probably the major elimination pathway. Human CYP3A had the greatest metabolic capability with other human P450s playing minor roles. Anlotinib exhibited large apparent volumes of distribution in rats (27.6±3.1 L/kg) and dogs (6.6±2.5 L/kg) and was highly bound in rat (97%), dog (96%), and human plasma (93%). In human plasma, anlotinib was predominantly bound to albumin and lipoproteins, rather than to α_1 -acid glycoprotein or γ -globulins. Concentrations of anlotinib in various tissue homogenates of rat and in those of tumor-bearing mouse were significantly higher than the associated plasma concentrations. Anlotinib exhibited limited *in vitro* potency to inhibit many human P450s, UDP-glucuronosyltransferases, and transporters, except for CYP3A4 and CYP2C9 (*in vitro* half maximum inhibitory concentrations, <1 μ mol/L). Based on early reported human pharmacokinetics, drug interaction indices were 0.16 for CYP3A4 and 0.02 for CYP2C9, suggesting that anlotinib had a low propensity to precipitate drug interactions on these enzymes. Anlotinib exhibits many pharmacokinetic characteristics similar to other tyrosine kinase inhibitors, except for terminal half-life, interactions with drug metabolizing enzymes and transporters, and plasma protein binding.

Keywords: anlotinib; tyrosine kinase inhibitor; absorption; distribution; metabolism; excretion; pharmacokinetics

Acta Pharmacologica Sinica (2018) 39: 1048–1063; doi: 10.1038/aps.2017.199; published online 5 Apr 2018

Introduction

Tyrosine kinases are key components of signal transduction pathways in the cell that relay information about conditions in the extracellular domain or the cytoplasm to pass on to the nucleus. Many tumor cells show abnormal activity of specific tyrosine kinases^[1]. To control such abnormal activity, a major effort has been made to discover small-molecule inhibitors that can block the phosphorylation mediated by the tyrosine kinases. Molecularly targeted therapies based on tyrosine

kinase inhibitors normally have a higher specificity toward tumor cells and less toxicity compared with cytotoxic chemotherapy. Clinical success of tyrosine kinase inhibitors in various advanced refractory tumors has established a paradigm for the treatment of tumors whose growth is acutely dependent on specific kinase targets^[2].

Anlotinib (AL3818), known as 1-[[[4-(4-fluoro-2-methyl-1H-indol-5-yloxy)-6-methoxyquinolin-7-yl]oxy]methyl] cyclopropanamine, is a novel multi-targeted tyrosine kinase inhibitor (details pending publication elsewhere). Anlotinib was found to suppress tumor development mainly through inhibition of VEGFR2 with a half maximum inhibitory concentration of 0.2 nmol/L; it inhibited tumor angiogenesis *in vitro* and *in vivo*. Oral administration of anlotinib resulted in

*To whom correspondence should be addressed.

E-mail chli@simm.ac.cn (Chuan LI);

niuwei@simm.ac.cn (Wei NIU)

Received 2017-04-24 Accepted 2017-12-19

reduced growth of several established human tumor xenografts in nude mice with little toxicity. A recent phase I study in patients with advanced refractory solid tumors (ClinicalTrials.gov Identifier: NCT01833923, at <https://clinicaltrials.gov/>) indicated that anlotinib, at the dose of 12 mg once daily at the 2-week on/1-week off schedule, displayed manageable toxicity, long circulation, and broad-spectrum antitumor potential^[3]. More recently, a randomized, double-blind, placebo-controlled, multi-centered phase III study in 437 patients with advanced non-small cell lung cancer (NCT02388919) suggested that treatment with anlotinib could be promising, given significantly prolonged median overall survival (9.6 months versus 6.3 months for the anlotinib-treated and control groups, respectively)^[4]. Currently, additional clinical studies are ongoing in a variety of malignancies including metastatic colorectal cancer (phase III; NCT02332499), medullary thyroid carcinoma (phase II; NCT02586350), differentiated thyroid carcinoma (phase II; NCT02586337), soft tissue sarcoma (phase II; NCT02449343), renal clear cell cancer (phase II; NCT02072031), gastric cancer (phase II; NCT02461407), esophageal squamous cell carcinoma (phase II; NCT02649361), and hepatocellular carcinoma (phase II; NCT02809534).

To evaluate the drug-like properties of anlotinib and to support associated safety and anticancer effect assessment in experimental animals and the follow-up clinical trials, pharmacokinetic studies in rats, tumor-bearing mice, and dogs, as well as associated *in vitro* studies, were performed to assess the compound's absorption, distribution, metabolism, and excretion. These experimental animal species were also used in nonclinical evaluation of safety or anticancer effects of anlotinib. This report describes findings from the preclinical pharmacokinetic studies.

Materials and methods

Chemicals and materials

Anlotinib (dihydrochloride form; purity >99%) used in animal studies and reference standard of anlotinib (dihydrochloride form; purity >99%) for analysis use were obtained from Jiangsu Chia-tai Tianqing Pharmaceutical Co, Ltd (Nanjing, China). For oral and intravenous administration to rats and dogs, anlotinib was dissolved in physiological saline to a variety of concentrations.

Sodium heparin, isoflurane, saline, and taurocholic acid were obtained from Sinopharm Chemical Reagent Co, Ltd (Shanghai, China). Pentobarbital was obtained from Shanghai Westang Biotechnology (Shanghai, China). Vardenafil hydrochloride, antipyrine, atenolol, imatinib mesylate, rhodamine 123, sulfasalazine, verapamil, MK571, novobiocin, Hank's balanced salt solution, nicotinamide adenine dinucleotide phosphate, glucose-6-phosphate, phenacetin, coumarin, bupropion, amodiaquine, diclofenac, (S)-mephentoin, dextrorphan, chlorzoxazone, gluco-6-phosphate monosodium salt, β -estradiol, trifluoperazine, 4-methylumbelliferone, β -estradiol-3- β -D-glucuronide, trifluoperazine-N- β -D-glucuronide, 4-methylumbelliferyl- β -D-glucuronide, atazanavir, hecogenin, phenylbutazone, niflumic acid, alamethicin,

Uridine 5'-diphosphoglucuronic acid (UDPGA), estradiol-17 β -D-glucuronide, estrone-3-sulfate, para-aminohippuric acid, tetraethylammonium, methotrexate, cimetidine, probenecid, rifampin, and ethyl acetate were obtained from Sigma-Aldrich (St Louis, MO, USA). Senkyunolides I were obtained from Shanghai Standard Technology (Shanghai, China). Tariquidar was obtained from Selleck (Houston, TX, USA). Ginsenoside Rg₁ and midazolam was obtained from the National Institutes for Food and Drug Control (Beijing, China). HPLC-grade acetonitrile, formic acid, and methanol were obtained from Merck (Darmstadt, Germany). HPLC-grade water was prepared using a Millipore Milli-Q integral water purifying system (Bedford, MA, USA).

Human colon carcinoma (Caco-2) cells and human embryonic kidney 293 (HEK-293) cells were obtained from American Type Culture Collection (Manassas, VA, USA). Dulbecco's modified Eagle's medium, penicillin-streptomycin, and non-essential amino acids were obtained from Gibco Invitrogen Cell Culture (Grand Island, NY, USA). Fetal bovine serum was obtained from Corning Gentest (Woburn, MA, USA). Pooled human liver microsomes, cDNA-expressed human cytochrome P450 (P450) enzymes (CYP1A2, CYP2A6, CYP2B6, CYP2C8, CYP2C9, CYP2C19, CYP2D6, CYP2E1, CYP3A4, and CYP3A5), and CYP enzymes high throughput inhibitor screening kits of CYP1A2/CEC, CYP2B6/EFC, CYP2C8/DBF, CYP2C9/MFC, CYP2C19/CEC, CYP2D6/AMMC, and CYP3A4/BFC were obtained from Corning Gentest. Baculovirus insect cell-expressed human uridine 5'-diphosphoglucuronosyltransferases (UGT1A1, UGT1A3, UGT1A4, UGT1A6, UGT1A9, UGT2B7, and UGT2B15) was obtained also from Corning Gentest. Rat liver microsomes and dog liver microsomes were prepared in house. Full open reading frames of cDNA for human organic anion-transporting polypeptide (OATP) 1B1, human OATP1B3, human organic anion transporter (OAT) 1, human OAT3, and human organic cation transporter (OCT) 2 were synthesized and subcloned into pcDNA 3.1(+) expression vectors by Invitrogen Life Technologies (Shanghai, China). Prior to the study, all expression plasmids were sequence-verified according to their GeneBank accession numbers (human OATP1B1, NM_006446; human OATP1B3, NM_019844; human OAT1, NM_004790; human OAT3, NM_004254; human OCT2, NM_003058). Inside-out membrane vesicles (5 mg protein/mL), prepared from insect cells expressing human multidrug resistance 1 (MDR1), multidrug resistance-associated protein 2 (MRP1), or human breast cancer resistance protein (BCRP), were purchased from Genomembrane (Kanazawa, Ishikawa Prefecture, Japan). Lyophilized albumin (prepared from human plasma; purity $\geq 95\%$), lyophilized α_1 -acid glycoprotein (prepared from human plasma; purity >95%), high density lipoproteins (prepared from human plasma; purity >95%), low density lipoproteins (prepared from human plasma; purity >95%), and very low density lipoproteins (prepared from human plasma; purity >95%) were obtained from Athens Research & Technology (Athens, GA, USA). γ -Globulins (prepared from human blood; purity >99%) were obtained from Sigma-Aldrich.

Spectra/Por1 2 RC dialysis membranes (cellulose tubing, 15 m×6.4 mm id) with a molecular weight cutoff of 12–14 kDa were obtained from Spectrum Laboratories Inc (Rancho Dominguez, CA, USA). Millicell-PCF filter inserts (0.4- μ m, 12-mm diameter) were obtained from Millipore (Bedford, MA, USA).

Experimental animals

All animal care and use complied with the Guidance for Ethical Treatment of Laboratory Animals (The Ministry of Science and Technology of China, 2006, at www.most.gov.cn/fggw/zfwj/zfwj2006). All animal studies were implemented according to protocols, which were reviewed and approved by the Institutional Animal Care and Use Committee at Shanghai Institute of Materia Medica (Shanghai, China). Male and female Sprague Dawley rats (230–270 g) were obtained from SIPPR-BK Laboratory Animal Co Ltd (Shanghai, China). Female Balb/cA nude mice (18–20 g) were obtained from Shanghai Laboratory Animal Center (Shanghai, China). Nude mice were inoculated subcutaneously with 5×10^6 human colon cancer SW620 cells to establish a human tumor xenograft; the tumor-bearing mice were used when the tumors reached a volume of 400–600 mm³. Male and female beagle dogs (7–9 kg) were obtained from School of Agriculture and Biology, Shanghai Jiao Tong University (Shanghai, China). The animals were maintained on controlled temperature (20–24 °C), relative humidity (40%–70%), and a 12-h cycle of light and dark. The animals were given commercial diets, except for an overnight fasting period before dosing, and filtered tap water *ad libitum*. The rats and mice were acclimated to the facilities for 1 week before use and the dogs for 2 weeks. A total of 118 rats, 60 nude mice, and 24 dogs were used in the experiments described here.

Rat studies

Rats were randomly assigned to four groups (five male and five female rats per group) to receive a single oral dose of anlotinib at 1.5, 3, or 6 mg/kg (via gavage) or a single intravenous dose at 1.5 mg/kg (from the tail vein). Serial blood samples (around 0.25 mL; before and 5, 15, and 30 min and 1, 2, 4, 6, 8, 11, and 24 h after dosing) were collected in heparinized tubes from the orbital sinuses of rats under isoflurane anesthesia and centrifuged at $1300 \times g$ for 10 min to yield plasma fractions.

Rats under isoflurane anesthesia were killed by bleeding from the abdominal aorta at 1, 4, 8, and 24 h (three male and three female rats per time point) after a single oral dose of anlotinib at 3 mg/kg. The blood of rats was collected in heparinized evacuated blood collection tubes and centrifuged to yield plasma fractions. The testicles (male only), ovaries (female only), wombs (female only), bladders, adiposes, kidneys, adrenal glands, spleens, pancreases, stomachs, small intestines, colons, livers, hearts, lungs, brains, skeletal muscles, and femur bones were excised from the rats, rinsed in ice-cold saline, blotted, and weighed. The collected tissues were homogenized in four-fold volume of ice-cold water, except for the ovary, adipose, bladder, and adrenal glands, which were homogenized in 9-, 9-, 19-, and 29-fold volumes of ice-cold water, respectively.

Three male and three female rats were housed singly in metabolic cages with the urine collection tubes frozen at -15°C during sample collection. Urine and feces samples were collected from rats before and 0–4, 4–10, and 10–24 h after a single intravenous dose of anlotinib at 1.5 mg/kg and weighed.

Three male and three female rats received in-house bile-duct-cannulation under pentobarbital anesthesia and were allowed to regain their preoperative body weights before use. Serial bile samples were collected before and 0–3, 3–6, 6–9, 9–12, 12–18, and 18–24 h after a single intravenous dose of anlotinib at 1.5 mg/kg and weighed.

All rat samples were stored at -70°C pending analysis.

Tumor-bearing mouse studies

Female tumor-bearing mice were randomly assigned to three groups (20 mice per group) to receive a single oral dose of anlotinib at 0.75, 1.5, or 3 mg/kg (via gavage). Mice under isoflurane anesthesia were killed by bleeding from the orbital sinus at 2, 4, 8, and 24 h (five mice per time point) after dosing. The blood of mice was collected in heparinized tubes and centrifuged to yield plasma fractions. The lungs, livers, kidneys, colons, and tumor tissues were excised from the mice, rinsed in ice-cold saline, blotted, and weighed. The collected tissues were homogenized in four-fold volume of ice-cold water, except for the lungs, which were homogenized in nine-fold volumes of ice-cold water.

All mouse samples were stored at -70°C pending analysis.

Dog study

Dogs were randomly assigned to four groups (three male and three female dogs per group) to receive a single oral dose of anlotinib at 0.5, 1, or 2 mg/kg (via gavage) or a single intravenous dose at 0.5 mg/kg (from left forelimb vein). Serial blood samples (around 0.5 mL; before and 5, 15, and 30 min and 1, 2, 4, 6, 8, 11, and 24 h after dosing) were collected in heparinized tubes from the right forelimb vein of dogs and centrifuged to yield plasma fractions.

All dog plasma samples were stored at -70°C pending analysis.

In vitro assessment of pharmacokinetic and related physicochemical properties

Binding of anlotinib in plasma was assessed by a method of equilibrium dialysis [10 h at 37°C ; using Spectra/Por1 2 RC dialysis membranes with a molecular weight cutoff of 12–14 kDa and phosphate buffered saline (pH 7.4) as dialysate]^[5]. Anlotinib was spiked into blank rat, dog, or human plasma to generate concentrations of 276, 552, and 1104 ng/mL. After completion of dialysis, the concentrations of anlotinib in the dialysate and plasma samples were measured. The unbound fraction in plasma (f_u) was calculated using the following equation:

$$f_u = (C_u/C_t) \times 100\% \quad (1)$$

where C_u is the concentration (ng/mL) of anlotinib in the dialysate compartment after completion of dialysis and C_t is the concentration (ng/mL) of anlotinib in the plasma compartment after completion of dialysis. To understand the proteins

responsible for the binding in human plasma, anlotinib, at the concentrations 100, 200, 400, and 800 ng/mL, was assessed in solutions of the isolated human plasma proteins albumin (600 $\mu\text{mol/L}$), α_1 -acid glycoprotein (10 $\mu\text{mol/L}$), γ -globulins (80 $\mu\text{mol/L}$), high density lipoproteins (10 $\mu\text{mol/L}$), low density lipoproteins (1 $\mu\text{mol/L}$), and very low density lipoproteins (0.1 $\mu\text{mol/L}$) using the equilibrium dialysis method. Imatinib was used as a control. The total binding constant (nK ; $L/\mu\text{mol}$) was calculated using the following equation^[6]:

$$nK = (C_t - C_u)/(C_u \times [P]) \quad (2)$$

where C_t is the concentration (ng/mL) of anlotinib in the solution of the isolated human plasma protein(s) after completion of dialysis, C_u is the concentration (ng/mL) of anlotinib in the dialysate compartment after completion of dialysis, and $[P]$ is the protein concentration in the solution of the isolated human plasma protein(s). An $nK_{\alpha_1\text{-acid-glycoprotein}}/nK_{\text{albumin}}$ ratio (nK ratio) was used to indicate comparative binding to α_1 -acid glycoprotein and to albumin; an nK ratio of <7.7 was not considered to be large enough for a tyrosine kinase inhibitor to compensate the high excess of plasma concentration of albumin (600 $\mu\text{mol/L}$) over α_1 -acid glycoprotein (20 $\mu\text{mol/L}$)^[7].

Membrane permeability of anlotinib was assessed using Caco-2 cell monolayers. Caco-2 cells were cultured as previously described^[8]. Caco-2 cell monolayers exhibited a transepithelial electrical resistance value of $>400 \Omega \cdot \text{cm}^2$. The applicability of the cell monolayers was also evaluated using antipyrine (control compound of high membrane permeability), atenolol (control compound of low membrane permeability), rhodamine 123 (probe substrate of MDR1), sulfasalazine [probe substrate of multidrug resistance-associated protein 2 (MRP2)], estrone-3-sulfate (probe substrate of BCRP), verapamil (specific inhibitor of MDR1), MK571 (specific inhibitor of MRP2 and BCRP), and novobiocin (specific inhibitor of BCRP) before use. Bidirectional transport experiments were conducted in triplicate at 10 $\mu\text{mol/L}$ for anlotinib in Hanks' balanced salt solution. After incubation at 37 °C, samples were collected from the receiver side at 60 min. Samples were also collected from the donor side at the last sampling time to determine recovery of anlotinib and the control compounds. The apparent permeability coefficient (P_{app}) expressed in cm/s was calculated using the following equation:

$$P_{\text{app}} = (\Delta Q/\Delta t)/(A \times C_0) \quad (3)$$

where $\Delta Q/\Delta t$ is the linear appearance rate of the test compounds on the receiver side in $\mu\text{mol/s}$; A is the surface area of the cell monolayer in cm^2 ; and C_0 is the initial concentration of the test compound on the donor compartment in $\mu\text{mol/L}$. According to our in-house Caco-2 cell monolayer data, compounds with P_{app} values $<0.2 \times 10^{-6}$, 0.2×10^{-6} – 2.8×10^{-6} , and $>2.8 \times 10^{-6}$ cm/s were defined to be of low, intermediate, and high permeability, respectively^[9]. An efflux ratio ($P_{\text{app,B-A}}/P_{\text{app,A-B}}$) was used to implicate possible involvement of transporter-mediated efflux, and an efflux ratio (EfR) >3 was considered to be a positive result.

Aqueous solubility of anlotinib in different media, including hydrochloric acid buffer at pH 1.7, acetate buffer at pH 4.6, and phosphate buffer at 6.5, was determined by an equilib-

rium shake flask thermodynamic solubility method^[10]. Anlotinib was added to 2–5 mL of buffer media in a vial, which was shaken for 48 h at 37 °C. Undissolved anlotinib was separated by centrifugation. The concentration of anlotinib in the supernatant was measured in triplicate.

LogD values of anlotinib at pH 1.7, 4.6, and 6.5 in octanol/buffer solution system were measured by a shake-flask method^[10]. After agitation for 36 h, concentration of anlotinib in the organic phase and the aqueous phase was measured in triplicate.

In vitro metabolism studies

To identify the human P450 isoforms that could mediate oxidation of anlotinib, a variety of cDNA-expressed human P450 enzymes (CYP1A2, CYP2A6, CYP2B6, CYP2C8, CYP2C9, CYP2C19, CYP2D6, CYP2E1, CYP3A4, and CYP3A5), fortified with NADPH, were incubated with 2 $\mu\text{mol/L}$ anlotinib at 37 °C for 60 min. The incubation was performed in duplicate and the enzyme concentration was 50 pmol P450/mL. After centrifugation at $3000 \times g$ for 10 min, the resulting supernatants were analyzed by liquid chromatography/mass spectrometry.

To compare interspecies difference in P450-mediated oxidation of anlotinib, the compound at the final concentration 2 $\mu\text{mol/L}$ were incubated with rat liver microsomes, dog liver microsomes, and human liver microsomes in presence of NADPH. The incubations were performed in duplicate at 37 °C for 3, 7.5, 15, 30, or 60 min. The incubation conditions were the same as those described by Hu *et al*^[11]. The interspecies differences were characterized with respect to metabolic stability and metabolite formation.

In vitro assessment of inhibitory effects of anlotinib on the activity of human drug metabolizing enzymes and that of human drug transporters

Potential for anlotinib to inhibit human P450 enzyme activity was evaluated using cDNA-expressed CYP1A2, CYP2B6, CYP2C8, CYP2C9, CYP2C19, CYP2D6, CYP3A4, and CYP3A5. 3-Cyano-7-ethoxycoumarin, 7-ethoxy-4-trifluoromethylcoumarin, dibenzylfluorescein, 7-methoxy-4-trifluoromethylcoumarin, 3-[2-(*N,N*-diethyl-*N*-methylamino)ethyl]-7-methoxy-4-methylcoumarin, 7-benzyloxy-trifluoromethylcoumarin, and midazolam were used as probe substrates for CYP1A2/CYP2C19, CYP2B6, CYP2C8, CYP2C9, CYP2D6, CYP3A4, and CYP3A5, respectively, and the concentrations of these probe substrates in incubation mixtures were 5.0/25.0, 2.5, 1.0, 75.0, 1.5, 50.0, and 2.0 $\mu\text{mol/L}$, respectively. Initially, anlotinib, at 100 $\mu\text{mol/L}$ in incubation mixture, was assessed in triplicate for its inhibitory effects on P450 enzymes' activity. When demonstrating $>50\%$ inhibition, the half maximal inhibitory concentration (IC_{50}) of anlotinib was determined for the P450 enzymes. Each incubation mixture consisted of anlotinib, the cDNA-expressed P450 enzyme, and the associated probe substrate. The negative control mixture contained 0.2% methanol in place of anlotinib, whereas the positive control mixture contained a positive inhibitor in place of anlotinib. Positive control inhibitors for CYP1A2, CYP2B6, CYP2C8, CYP2C9,

CYP2C19, CYP2D6, and CYP3A4/CYP3A5 were furafylline, tranlycypromine, quercetin, sulfaphenazole, tranlycypromine, quinidine, and ketoconazole, respectively. The incubation mixture was equilibrated for 10 min before initiating the reaction by adding an NADPH-generating system, which comprised 3.3 mmol/L magnesium chloride, 3.3 mmol/L of glucose-6-phosphate, 0.5 U/mL glucose-6-phosphate dehydrogenase, and 1.3 mmol/L NADP. Incubation times were 10, 15, 30, 40, and 45 min for the CYP3A5-, CYP1A2-, CYP2B6-/CYP2C19-/CYP2D6-/CYP3A4-, CYP2C8-, and CYP2C9-mediated reactions, respectively. Enzymatic reactions were terminated with an equal volume of ice-cold acetonitrile, except for CYP2C8 using an equal volume of 2 mol/L sodium hydroxide solution to terminate the reaction followed by incubation at 37°C for 2 h. A SpectraMax M2 microplate reader (Molecular Devices, Sunnyvale, CA, USA) was used to measure the fluorescent metabolites of the probe substrates at the selected excitation/emission wavelengths, *ie*, 410/460, 409/530, 485/538, and 390/460 nm/nm, for 3-cyano-7-hydroxycoumarin, 7-hydroxy-4-trifluoromethylcoumarin, fluorescein, and 7-hydroxycoumarin/3-[2-(*N,N*-diethylamino)ethyl]-7-hydroxy-4-methylcoumarin, metabolites of the probe substrates for CYP1A2/CYP2C19, CYP2B6/CYP2C9/CYP3A4, CYP2C8, and CYP2D6, respectively. A liquid chromatography/mass spectrometry-based method was used to analyze 1'-hydroxymidazolam, the metabolite of the probe substrate midazolam for CYP3A5.

Potential for anlotinib to inhibit human UGT enzyme activity was evaluated using cDNA-expressed UGT1A1, UGT1A3, UGT1A4, UGT1A6, UGT1A9, UGT2B7, and UGT2B15. β -Estradiol, 4-methylumbelliferone, trifluoperazine, and senkyunolide I were used as probe substrates for UGT1A1, UGT1A3/UGT1A6/UGT1A9/UGT2B7, UGT1A4, and UGT2B15, respectively, and the concentrations of these probe substrates in incubation mixtures were 20, 1000/100/10/300, 40, and 20 μ mol/L, respectively. Initially, anlotinib, at 100 μ mol/L in incubation mixture, was assessed in triplicate for its inhibitory effects on UGT enzymes' activity. When demonstrating >50% inhibition, the half maximal inhibitory concentration (IC_{50}) of anlotinib was determined for the UGT enzymes. Each incubation mixture consisted of anlotinib, the cDNA-expressed UGT enzyme, alamethicin, and the associated probe substrate. The negative control mixture contained 0.2% methanol in place of anlotinib, whereas the positive control mixture contained a positive inhibitor in place of anlotinib. Positive control inhibitors for UGT1A1/UGT1A9, UGT1A3, UGT1A4, UGT1A6, and UGT2B7/UGT2B15 were niflumic acid, atazanavir, hecogenin, phenylbutazone, and diclofenac, respectively. The incubation mixture was equilibrated for 5 min before initiating the reaction by adding UDPGA. Incubation times were 30, 75, 20, 15, 120, and 20 min the UGT1A1-/UGT1A6-, UGT1A3-, UGT1A4-, UGT1A9-, UGT2B7-, and UGT2B15-mediated enzymatic reactions, respectively. These reactions were stopped by adding two volumes of ice-cold methanol followed by centrifugation at 1000 \times g for 10 min. The supernatants were analyzed, by liquid chromatography/

mass spectrometry, to determine the quantity of the formed glucuronides, *ie*, E3G, 4-MUG, TFGP, and senkyunolide I-7-*O*- β -glucuronide for UGT1A1, UGT1A3/UGT1A6/UGT1A9/UGT2B7, UGT1A4, and UGT2B15, respectively.

To evaluate potential for anlotinib to inhibit human transporter activity, human organic anion-transporting polypeptide (OATP) 1B1, OATP1B3, human organic cation transporter (OCT) 2, human organic anion transporter (OAT) 1 and OAT3 plasmids and the empty vector were introduced separately into the HEK-293 cells with Lipofectamine 2000 transfection reagent (Invitrogen, Carlsbad, CA, USA) as previously described^[12, 13]. Initially, anlotinib, at 100 μ mol/L in incubation mixture, was assessed for its inhibitory effects on activity of OATP1B1, OATP1B3, OCT2, OAT1, and OAT3, and the probe substrates used were estradiol-17 β -*D*-glucuronide, para-aminohippuric acid, tetraethylammonium, and estrone-3-sulfate, respectively, with a concentration of 10 μ mol/L in incubation mixtures for all. When demonstrating >50% inhibition, the IC_{50} of anlotinib was determined for the transporter. All experiments were run in triplicate. Concentrations of the probe substrates in the cells after incubation were determined by liquid chromatography/mass spectrometry.

Inhibitory effects of anlotinib on activity of human MDR1, MRP1, and BCRP were evaluated using membrane vesicles expressing the transporters and ginsenoside Rg₁, estradiol-17 β -*D*-glucuronide, and methotrexate, both at 10 μ mol/L in incubation mixtures, were used as probe substrates, respectively. Initially, anlotinib, at 100 μ mol/L in incubation mixture, was assessed for its inhibitory effects on activity of the transporters. When demonstrating >50% inhibition, the IC_{50} of anlotinib was determined for the transporter. The details of vesicular transport methods with the probe substrates were described by Jiang *et al*^[12], and all experiments were run in triplicate. Quantity of the probe substrates trapped inside the vesicles after incubation was determined by liquid chromatography/mass spectrometry.

LC-MS-based bioanalytical assays

An Applied Biosystems Sciex API 4000 Q Trap mass spectrometer (Toronto, Ontario, Canada), interfaced via a Turbo V ion source with a Waters Acquity UPLC separation module (Milford, MA, USA), was used for analysis of unchanged and metabolized anlotinib in biological matrices. The chromatographic separation was achieved on a 5.0 μ m Agilent Eclipse Plus C₁₈ column (50 mm \times 2.1 mm id; Agilent, Chadds Ford, PA, USA). The mobile phase, delivered at 0.25 mL/min, consisted of acetonitrile/water (1:99, *v/v*, containing 5 mmol/L formic acid; solvent A) and acetonitrile/water (99:1, *v/v*, containing 5 mmol/L formic acid; solvent B). For quantification analysis, a gradient program was used, which consisted of 0–2 min from 5% B to 80% B, 2–3 min at 80% B, and 3–7 min at 5% B. For metabolite detection and characterization, a binary gradient method was used, *ie*, 0–10 min from 5% B to 25% B, 10–13 min from 25% B to 100% B, and 13–18 min at 5% B.

For quantification of anlotinib in various biological matrices, the instrument parameters for mass spectrometry were

optimized in the positive ion mode to maximize generation of protonated ions for anlotinib and the internal standard vardenafil and to yield their characteristic product ions. The precursor-to-product ion pairs used for multiple-reaction-monitoring of anlotinib and the internal standard were m/z 408→339 (the optimized collision energy, 23 V) and 489→151 (69 V), respectively. Matrix-matched calibration curves were constructed using weighted ($1/X$) linear regression of the peak area of anlotinib to internal standard (Y) against the corresponding nominal anlotinib concentration (X , ng/mL). The assays were validated according to the China FDA guidance on bioanalytical validation (2014; <http://www.sda.gov.cn/WS01/CL1616/101019.html>) to demonstrate their reliability and reproducibility for the intended use. The assay's lower limits of quantification of anlotinib were 0.2–11.6 ng/mL. The intra-batch accuracy and precision were 85.2%–108.8% and 1.7%–16.0%, respectively, while inter-batch values were 99.0%–101.6% and 1.6%–5.3%, respectively.

Detection of anlotinib metabolites in biological matrices was facilitated by using the PALLAS MetabolExpert 3.7 software (CompuDrug International, Sedona, AZ, USA) and Accelrys metabolite database (version 2015.1; San Diego, CA, USA) to predict possible metabolic pathways of anlotinib and to generate a list of its phases I and II metabolite candidates with information regarding molecular mass gains and losses between metabolites and the parent compound. The detected anlotinib metabolites were initially characterized according to their fragmentation profiles compared with that of the parent compound or their diagnostic fragment ions or neutral losses. In addition, characterization of *in vivo* oxidized metabolites of anlotinib was also based on comparing their liquid chromatograph/mass spectrometry profiles with those of the respective *in vitro* metabolites formed by simulating the *in vivo* metabolic reactions using the same parent compound purified anlotinib, human P450 enzymes, and the cofactor NADPH.

For quantification of anlotinib in biological matrices, the samples were extracted with ethyl acetate. After centrifugation, the ethyl acetate extracts were reduced to dryness under a stream of N_2 gas and the resulting residues were reconstituted in 50% methanol before analysis. For detection and characterization of anlotinib metabolites in biological matrices, the samples were precipitated with methanol. After centrifugation, the supernatants were applied to analysis.

Data processing

Plasma pharmacokinetic parameters of anlotinib were determined using non-compartmental analysis with Kinetica software (version 5.0; Thermo Scientific, Philadelphia, PA, USA). The maximum concentration (C_{max}) and the time taken to achieve the peak concentration (T_{peak}) after oral dose were obtained directly from the data without interpolation. The area under the concentration-time curve up to the last measured point in time (AUC_{0-t}) was calculated using the trapezoidal rule. The total plasma clearance ($CL_{tot,p}$) was estimated by dividing the dose by the $AUC_{0-\infty}$ and the distribution volume at steady state (V_{ss}) was estimated by multiplying the $CL_{tot,p}$

by the mean residence time (MRT). The $t_{1/2}$ was calculated using the relationship $0.693/k_e$. Oral bioavailability (F) was calculated by dividing the AUC_{oral} by the $AUC_{intravenous}$. Dose proportionality was assessed using the regression of log-transformed data (the Power Model), and the criteria was calculated according to a method by Smith *et al.*^[14]. The fractions of dose excreted into urine (f_{e-U}), feces (f_{e-F}), and into bile (f_{e-B}) were established using the relationships $Cum.A_{e-U}/Dose$, $Cum.A_{e-F}/Dose$, and $Cum.A_{e-B}/Dose$, respectively. IC_{50} values, in $\mu\text{mol/L}$, for inhibiting activity of a certain drug metabolizing enzyme or transporter were calculated using GraFit software (version 5.0; Erithacus Software, Surrey, UK). All data are expressed as the mean±standard deviation. Statistical analysis was performed using IBM SPSS Statistics software (version 19.0; IBM, Somers, NY, USA). A P value <0.05 was considered statistically significant.

Results

Plasma pharmacokinetics of anlotinib in rats and in dogs

Mean plasma concentrations of anlotinib over time after a single dose of anlotinib in rats and dogs are shown in Figure 1; the plasma pharmacokinetic parameters of anlotinib are summarized in Table 1. After oral administration, levels of systemic exposure to anlotinib, i.e., plasma maximum concentration (C_{max}) and area under the plasma concentration-time curve up to 24 h (AUC_{0-24h}), in female rats tended to be greater than those in male rats at the tested dose range 1.5–6 mg/kg, while gender differences in plasma C_{max} and AUC_{0-24h} of anlotinib were not significant in dogs at the dose range 0.5–2 mg/kg. The plasma C_{max} and AUC_{0-24h} increased as the anlotinib dose increased in an over-proportional manner in rats and dogs (Table 2). Anlotinib was highly bound in rat, dog, and human plasma with unbound fractions in plasma (f_u) of 2.9%, 4.0%, and 7.3%, respectively. These f_u values were independent of total plasma concentration of anlotinib, suggesting that such total concentration of anlotinib is a good measure of the changes in its unbound concentration in plasma for the species. As shown in Table 3, anlotinib exhibited binding affinity for α_1 -acid glycoprotein similar to imatinib, another tyrosine kinase inhibitor. However, it exhibited substantially higher affinity for albumin than imatinib. Unlike imatinib with an $nK_{\alpha_1\text{-acid-glycoprotein}}/nK_{\text{albumin}}$ ratio of 92.0, such a ratio for anlotinib was 0.9 (<7.7), suggesting the high excess of plasma concentration of albumin (600 $\mu\text{mol/L}$) over α_1 -acid glycoprotein (20 $\mu\text{mol/L}$) could not be compensated for circulating anlotinib in humans. It is worth mentioning that anlotinib exhibited notably higher affinity for plasma lipoproteins, particularly for low density lipoproteins and very low density lipoproteins, than for albumin and α_1 -acid glycoprotein. After oral administration, anlotinib was rapidly absorbed from the gastrointestinal tract in rats and dogs (Figure 1). Dogs tended to exhibit greater oral bioavailability (F) of anlotinib than rats. Terminal half-lives ($t_{1/2}$) of anlotinib in rats and dogs after intravenous administration were comparable with the respective $t_{1/2}$ values after oral administration. Dogs exhibited a longer mean $t_{1/2}$ of anlotinib than rats. This $t_{1/2}$ difference

appeared to be attributed mainly to interspecies difference in total plasma clearance ($CL_{tot,p}$). Anlotinib's mean apparent volume of distribution at steady state (V_{SS}) in rats was 40 times as much as the rat volume of total body water and the value of V_{SS} in dogs was 12 times as much as the dog volume of total body water^[15], suggesting the compound was distributed widely into various body fluids and tissues. In rats that

received an intravenous dose of anlotinib, only small amounts of the unchanged compound were excreted into urine, bile, and feces (Table 1), suggesting that metabolism was the major elimination route of anlotinib.

Intestinal absorption-related properties of anlotinib

Intestinal absorption of a drug is a combined result of its solu-

Table 1. Pharmacokinetics of anlotinib in rats and dogs after a single dose of anlotinib.

Pharmacokinetic parameter	Intravenous dose		Oral low dose		Oral intermediate dose		Oral high dose	
	Male	Female	Male	Female	Male	Female	Male	Female
Rat data (intravenous dose, 1.5 mg/kg; oral dose, 1.5, 3, and 6 mg/kg)								
Rat number/group	5	5	5	3	5	5	5	5
C_{max} (ng/mL)	122±13	138±18	7±2	14±5*	15±5	22±10	42±25	129±83
$AUC_{0-24 h}$ (ng·h/mL)	226±41	326±26	81±5	134±41*	124±42	210±78	331±87	758±179*
$t_{1/2}$ (h)	3.8±1.0	6.4±0.8	4.1±0.3	4.0±0.5	4.4±1.6	3.7±0.4	5.7±3.1	4.2±0.4
V_{SS} (L/kg)	25.4±3.9	28.7±2.7	—	—	—	—	—	—
$CL_{tot,p}$ (L·h ⁻¹ ·kg ⁻¹)	6.34±1.12	4.37±0.40	—	—	—	—	—	—
F (%)	—	—	35.7±2.0	41.0±12.7	27.5±9.4	32.2±11.9	36.6±9.7	58.1±13.7
f_{e-U} (%)	0.79±0.16	0.40±0.28	—	—	—	—	—	—
f_{e-B} (%)	0.58±0.11	0.39±0.08	—	—	—	—	—	—
f_{e-F} (%)	3.41±0.38	2.62±0.80	—	—	—	—	—	—
Dog data (intravenous dose, 0.5 mg/kg; oral dose, 0.5, 1, and 2 mg/kg)								
Dog number/group	3	3	3	3	3	3	3	3
C_{max} (ng/mL)	141±34	136±43	49±15	49±16	85±17	88±12	222±68	363±65
$AUC_{0-24 h}$ (ng·h/mL)	1187±85	1264±222	638±118	707±299	1130±43.7	1048±166	2341±364	3909±1181
$t_{1/2}$ (h)	24.0±16.6	21.6±4.9	46.3±16.0	24.8±18.0	14.4±3.2	27.0±13.7	18.6±3.0	12.9±5.0
V_{SS} (L/kg)	6.8±1.9	6.3±3.5	—	—	—	—	—	—
$CL_{tot,p}$ (L·h ⁻¹ ·kg ⁻¹)	0.38±0.09	0.42±0.04	—	—	—	—	—	—
F (%)	—	—	53.7±10.0	55.9±23.7	47.6±1.8	41.4±6.6	49.3±7.7	77.3±23.4

C_{max} : maximum plasma concentration; $AUC_{0-24 h}$: area under plasma concentration-time curve from zero up to 24 h; $t_{1/2}$: terminal half-life; V_{SS} : distribution volume at steady state; $CL_{tot,p}$: total plasma clearance; F : oral bioavailability; f_{e-U} : fractions of dose excreted into urine; f_{e-B} : fractions of dose excreted into bile; f_{e-F} : fractions of dose excreted into feces. * P <0.05.

Table 2. Results of dose proportionality assessment for anlotinib in rats and dogs after an oral dose of anlotinib.

Pharmacokinetic parameter	r	P	Slope (90% CI)	Conclusion
Male rats (Test doses: 1.5, 3, and 6 mg/kg; $n=4, 5, 5$, respectively)				
C_{max}	0.85	0.0001	1.12 (0.76, 1.48)	Inconclusive
$AUC_{0-24 h}$	0.96	0.0000002	1.04 (0.88, 1.21)	Inconclusive
Female rats (Test doses: 1.5, 3, and 6 mg/kg; $n=3, 5, 5$, respectively)				
C_{max}	0.83	0.0002	1.64 (1.10, 2.19)	Inconclusive
$AUC_{0-24 h}$	0.89	0.00004	1.33 (0.97, 1.69)	Inconclusive
Male dogs (Test doses: 0.5, 1, and 2 mg/kg; $n=3, 3, 3$, respectively)				
C_{max}	0.93	0.0003	1.09 (0.78, 1.40)	Inconclusive
$AUC_{0-24 h}$	0.98	0.000008	0.94 (0.79, 1.10)	Inconclusive
Female dogs (Test doses: 0.5, 1, and 2 mg/kg; $n=3, 3, 3$, respectively)				
C_{max}	0.95	0.00008	1.46 (1.12, 1.80)	Inconclusive
$AUC_{0-24 h}$	0.91	0.0006	1.25 (0.85, 1.66)	Inconclusive

Critical intervals were 0.84–1.16. The term r denotes the correlation coefficient. Correlations were statistically significant with a P <0.05. The term "linear" was concluded statistically if the 90% confidence interval (90% CI) for slope was contained completely within the critical interval; "inconclusive" was concluded statistically if the 90% CI lay partly within the critical interval; "nonlinear" was concluded statistically if the 90% CI was entirely outside the critical interval. C_{max} : maximum plasma concentration; $AUC_{0-24 h}$: area under plasma concentration-time curve from zero up to 24 h.

Table 3. Binding of anlotinib and the control compound imatinib to individual proteins of human plasma and protein/albumin nK ratios.

Human plasma protein	Protein concentration in human plasma (μmol/L)	Binding percentage in isolated plasma protein solution (%)	nK (L/μmol)	Plasma protein/albumin nK ratio	Relative binding capability (%)
<i>Anlotinib</i>					
Albumin	600	99.9±0.0	1.32	1.00	57.3
α ₁ -Acid glycoprotein	10	93.7±1.0	1.24	1.02	0.9
γ-Globulins	80	32.5±12.2	0.01	0.01	0.1
High density lipoproteins	10	99.6±0.2	12.47	9.45	9.0
Low density lipoproteins	1	99.7±0.1	286.60	217.12	20.7
Very low density lipoproteins	0.1	99.5±0.1	1655.60	1254.24	12.0
<i>Imatinib (control)</i>					
Albumin	600	89.1±1.5	0.01	1.00	24.5
α ₁ -Acid glycoprotein	10	91.7±1.9	0.92	76.92	31.5
γ-Globulins	80	40.9±2.9	0.01	0.83	2.7
High density lipoproteins	10	82.1±5.9	0.39	32.33	13.2
Low density lipoproteins	1	82.9±1.6	5.39	449.17	18.4
Very low density lipoproteins	0.1	75.0±4.7	28.45	2371.00	9.7

Relative binding capability is calculated by $\{(nK_{\text{protein}} \times [\text{protein}]) / (nK_{\text{albumin}} \times [\text{albumin}] + nK_{\alpha_1\text{-acid glycoprotein}} \times [\alpha_1\text{-acid glycoprotein}] + nK_{\gamma\text{-globulins}} \times [\gamma\text{-globulins}] + nK_{\text{high density lipoproteins}} \times [\text{high density lipoproteins}] + nK_{\text{low density lipoproteins}} \times [\text{low density lipoproteins}] + nK_{\text{very low density lipoproteins}} \times [\text{very low density lipoproteins}])\} \times 100\%$.

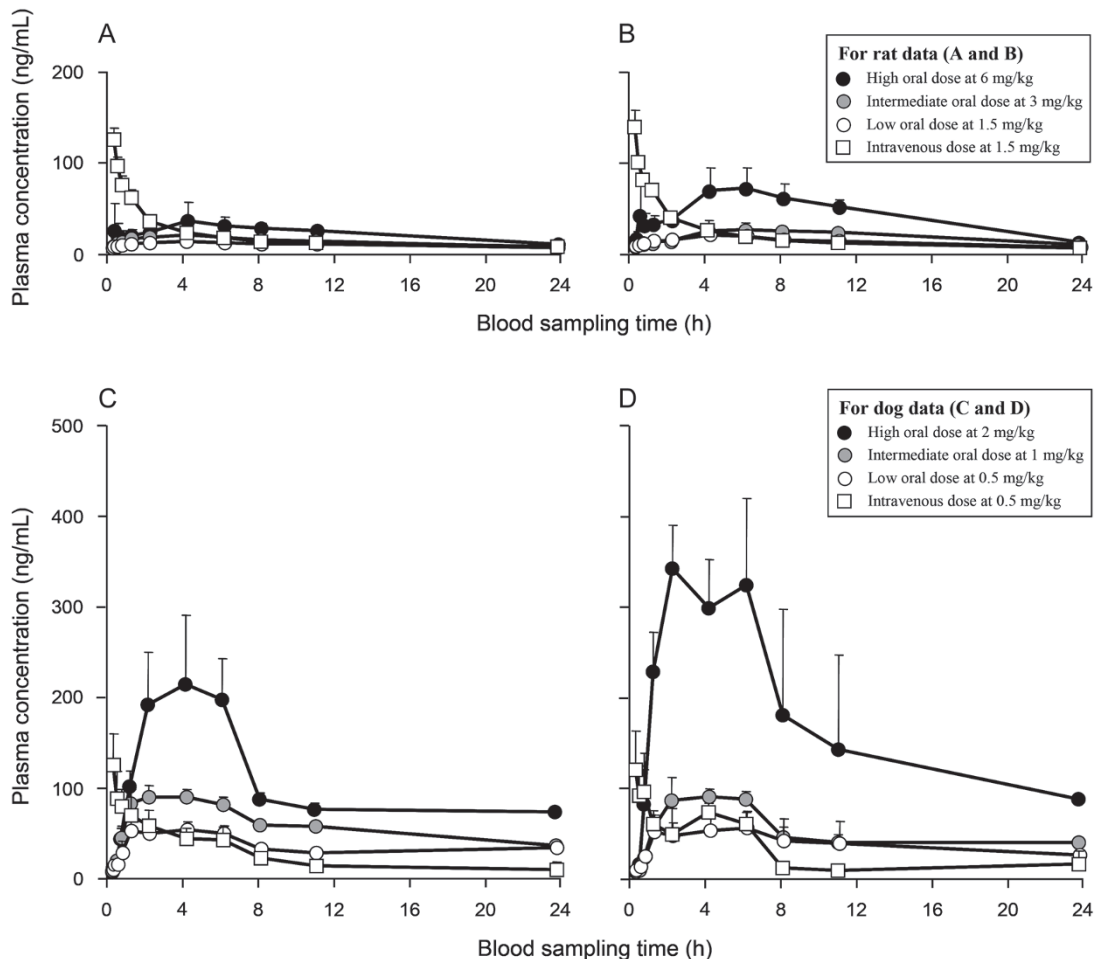


Figure 1. Mean plasma concentrations of anlotinib over time in male rats (A), female rats (B), male dogs (C), and female dogs (D) after an oral or intravenous dose of anlotinib.

bility in gastrointestinal fluids, membrane permeability, and substrate specificity to efflux system of the intestinal epithelia. Anlotinib exhibited pH-dependent aqueous solubility, *ie*, >1 g/mL at pH 1.7 (the stomach), 114 µg/mL at pH 4.6 (the duodenum), and 0.89 µg/mL at pH 6.5 (the jejunum and the ileum). The solubility values of anlotinib at pH 1.7 and 4.6 were greater than the compound's minimum solubility necessary to achieve adequate intestinal absorption at the dose 6 mg/kg, but the solubility value at pH 6.5 was lower than the minimum solubility. The minimum solubility was deduced according to a bar chart, by Lipinski, that depicts the minimum solubility for compounds with low, medium, and high permeability at doses of 0.1, 1, and 10 mg/kg^[16]. Anlotinib exhibited good membrane permeability across Caco-2 cell monolayers, expressing MDR1, MRP2, and BCRP, with a mean apparent permeability coefficient (P_{app}) of 3.5×10^{-6} cm/s. The compound exhibited a mean efflux ratio (Efr) of 0.91 ± 0.22 , suggesting that its transport across the cell monolayer did not affected by the apical efflux transporters in Caco-2 cells (Supplementary Figure S1). Physicochemical properties of anlotinib (predicted using ACD/Percepta; Toronto, Ontario, Canada), *ie*, molecular mass (407 Da; favorable value, <500 Da), hydrogen-bonding capacity (HBA+HBD, 6+3; <12), topo-

logical polar surface area (TPSA, 82.4 Å²; <140 Å²), and molecular flexibility (NROTB, 6; <10), supported its good membrane permeability. Measured LogD values were -0.89 at pH 1.7, 2.10 at pH 4.6, and 2.38 at pH 6.5 (favorable range, 0–5).

Tissue distribution of anlotinib in rats and tumor-bearing mice

Levels of various tissue exposures to anlotinib (measured using associated tissue homogenate samples) in rats and tumor-bearing mice after an oral dose of the compound were significantly higher than the associated systemic exposure level (Figure 2). In rats, the lung exhibited the highest exposure level, which was 197 times as high as the systemic exposure level. Meanwhile, the rat liver, kidneys, and heart also exhibited high exposure levels, which were 49, 54, and 32 times as much as the systemic exposure level. Anlotinib penetrated the rat brain, with a brain homogenate AUC_{0-24h} level comparable to the associated plasma level. In tumor-bearing mice, the level of tumor tissue exposure to the compound increased as the dose increased; it was 13 times as high as the systemic exposure level.

Metabolism of anlotinib

Because neither hepatobiliary nor renal excretion of

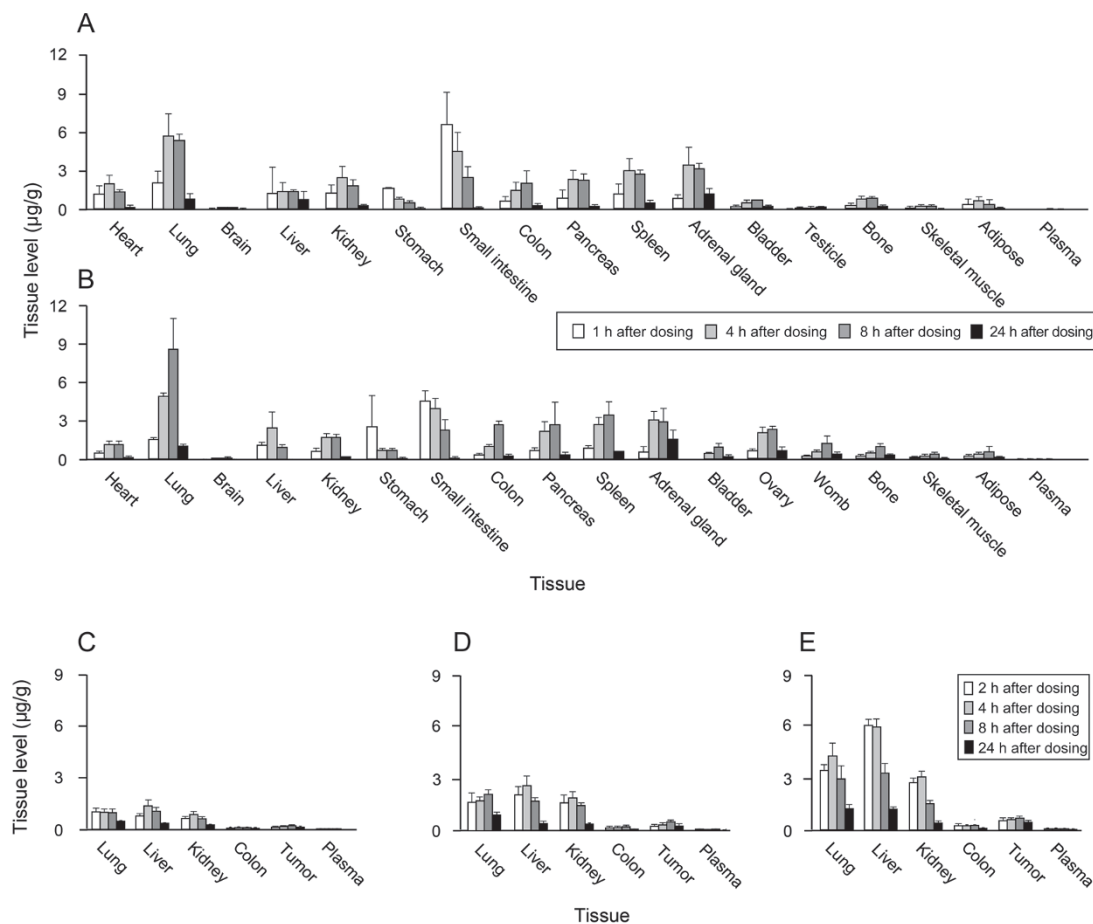


Figure 2. Tissue distribution of anlotinib in male rats (A), female rats (B), and female tumor-bearing mice (C–E) after an oral dose of anlotinib (3 mg/kg for rats, 0.75, 1.5, and 3 mg/kg for tumor-bearing mice).

unchanged compound was the main elimination route, metabolites of anlotinib in rat and dog samples were detected and characterized. As a result, a total of 12 anlotinib metabolites (**M1–M12**) were detected in the plasma, bile, urine, and feces samples of rats after dosing (Table 4). Eight of the metabolites, *ie*, **M2**, **M4**, **M5**, **M6**, **M8**, **M9**, **M10**, and **M11**, were found in plasma. All these metabolites occurred in rat bile and urine samples, except for **M7** and **M11**, which occurred only in rat bile samples. In dogs, a total of 5 metabolites of anlotinib were detected in plasma samples; they were **M4**, **M8**, **M9**, **M10**, and **M11**. After liquid chromatography/mass spectrometry-based characterization of these metabolites, metabolic pathways of anlotinib were proposed (Figure 3). The major metabolic pathways of anlotinib in rats were probably the hydroxylation to form **M10** and **M11** and the dealkylation to form **M8**. The metabolites **M10** and **M11** were two major plasma metabolites of anlotinib in rats, while **M8** was further glucuronized to

form **M6**, a major plasma and biliary metabolite of anlotinib. To further characterize these metabolic pathways, *in vitro* metabolism studies were performed for anlotinib. As a result, multiple human cytochrome P450 enzymes, *ie*, CYP1A2, CYP2A6, CYP2B6, CYP2C8, CYP2C9, CYP2C19, CYP2D6, CYP2E1, CYP3A4, and CYP3A5, were found to be able to mediate the oxidation of anlotinib to form **M10**, **M11**, and **M8** (Figure 4A). Among these enzymes were CYP3A4 and CYP3A5 that exhibited the greatest metabolic capabilities. As shown in Figure 4B, the metabolites **M10**, **M11**, and **M8** were also detected in samples of anlotinib after being incubated with NADPH-fortified rat liver microsomes, dog liver microsomes, and human liver microsomes under the same conditions. The total amounts of metabolites formed were different for the tested liver microsomes of different species, suggesting the highest oxidation rate by rat liver microsomes followed by dog liver microsomes, and then by human liver microsomes.

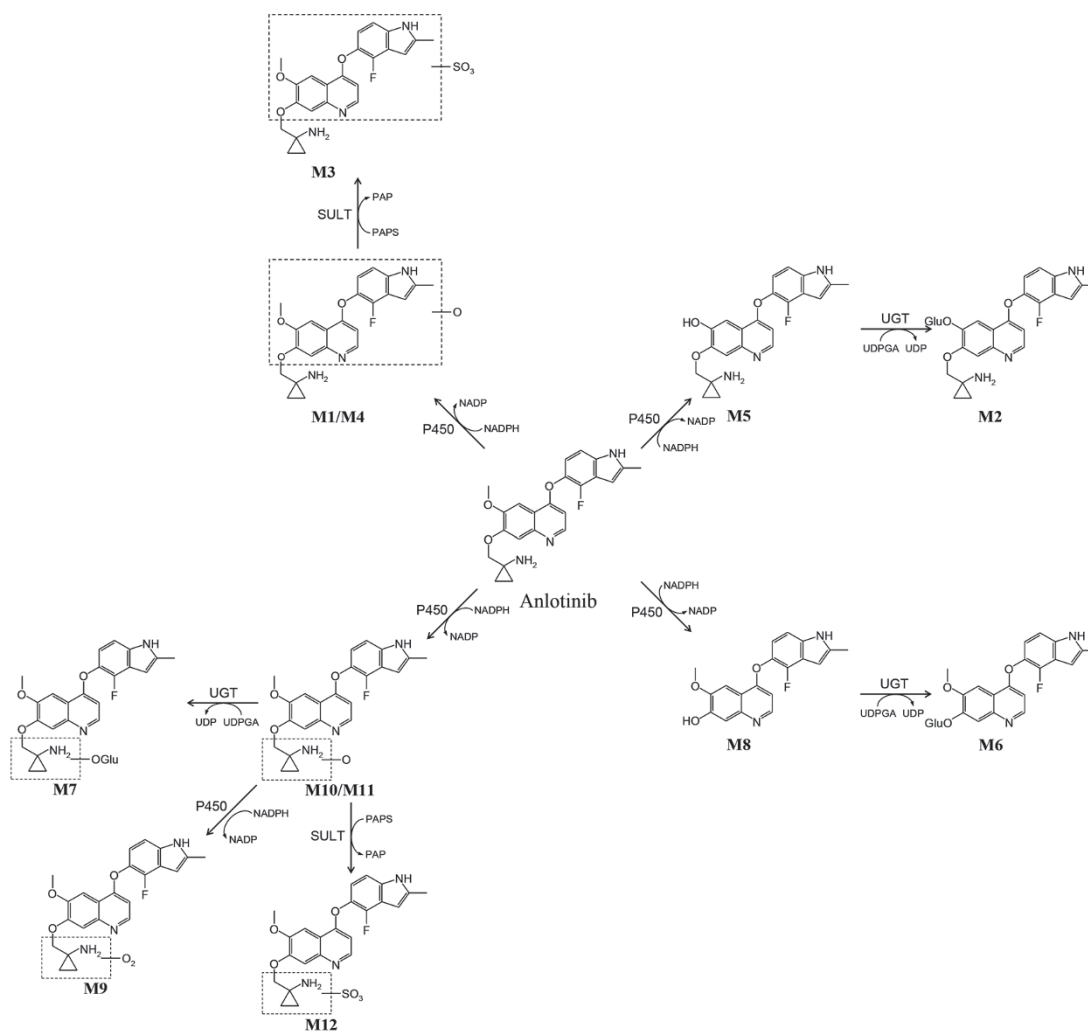


Figure 3. Proposed metabolic pathways of anlotinib. P450, cytochrome P450 enzymes; NADPH, reduced β -nicotinamide adenine dinucleotide phosphate; NADP, β -nicotinamide adenine dinucleotide phosphate; UGT, uridine 5'-diphosphoglucuronosyltransferase; UDPGA, uridine 5'-diphosphoglucuronic acid; UDP, uridine 5'-diphosphate; SULT, sulfotransferase; PAPS, 3'-phosphoadenosine-5'-phosphosulphate; PAP, 3'-phosphoadenosine-5'-phosphate; Glu, glucuronosyl.

Table 4. Liquid chromatography/mass spectrometry-based detection and characterization of metabolites of anlotinib in rats and dogs after dosing.

Liquid chromatography/mass spectrometry profile						
ID	Retention time (min)	Protonated molecule (<i>m/z</i>)	Characteristic fragment ion (neutral loss) from the protonated molecule (<i>m/z</i>) (Da)	Molecular formula	Metabolic reaction type	Presence in rat sample Presence in dog sample
Anlotinib	9.2	408	339 [M+H-69] ⁺ , 304 [M+H-104] ⁺ , 276 [M+H-132] ⁺ , 248 [M+H-160] ⁺	C ₂₃ H ₂₂ FN ₃ O ₃	-	Plasma, bile, urine, feces Plasma
M1	5.7	424 (408+16)	355 [M+H-69] ⁺ , 320 [M+H-104] ⁺ , 276 [M+H-(132+16)] ⁺ , 248 [M+H-(160+16)] ⁺	C ₂₃ H ₂₂ FN ₃ O ₄	Oxidation of anlotinib	Bile, urine Not detected
M2	5.7	570 (408-14+176)	394 [M+H-176] ⁺ , 325 [M+H-176-69] ⁺ (176)	C ₂₈ H ₂₈ FN ₃ O ₉	Glucuronidation of M5	Plasma, bile, urine Not detected
M3	6.0	504 (408+16+80)	424 [M+H-80] ⁺ , 355 [M+H-80-69] ⁺ (80)	C ₂₃ H ₂₂ FN ₃ SO ₇	Sulfation of M1 or M4	Bile, urine Not detected
M4	6.3	424 (408+16)	355 [M+H-69] ⁺ , 320 [M+H-104] ⁺ , 276 [M+H-(132+16)] ⁺ , 248 [M+H-(160+16)] ⁺	C ₂₃ H ₂₂ FN ₃ O ₄	Oxidation of anlotinib	Plasma, bile, urine, feces Plasma
M5	8.4	394 (408-14)	325 [M+H-69] ⁺ ; 276 [M+H-(132-14)] ⁺	C ₂₂ H ₂₀ FN ₃ O ₃	Oxidation of anlotinib	Plasma, bile, urine Not detected
M6	10.0	515 (408-69+176)	339 [M+H-176] ⁺ , 304 [M+H-176-(104-69)] ⁺ , 248 [M+H-176-(160-69)] ⁺ (176)	C ₂₅ H ₂₃ FN ₂ O ₉	Glucuronidation of M8	Plasma, bile, urine Not detected
M7	11.4	600 (408+16+176)	424 [M+H-176] ⁺ , 355 [M+H-176-69] ⁺ , (176)	C ₂₉ H ₃₀ FN ₃ O ₁₀	Glucuronidation of M10 or M11	Bile Not detected
M8	11.6	339 (408-69)	304 [M+H-(104-69)] ⁺ , 276 [M+H-(132-69)] ⁺ , 248 [M+H-(160-69)] ⁺	C ₁₉ H ₁₅ FN ₂ O ₃	Oxidation of anlotinib	Plasma, bile, urine, feces Plasma
M9	11.6	440 (408+16+16)	355 [M+H-(69+16)] ⁺ , 339 [M+H-(69+16+16)] ⁺	C ₂₃ H ₂₂ FN ₃ O ₅	Oxidation of M10 or M11	Plasma, bile, urine, feces Plasma
M10	11.7	424 (408+16)	339 [M+H-(69+16)] ⁺ , 304 [M+H-(104+16)] ⁺ , 276 [M+H-(132+16)] ⁺ , 248 [M+H-(160+16)] ⁺	C ₂₃ H ₂₂ FN ₃ O ₄	Oxidation of anlotinib	Plasma, bile, urine, feces Plasma
M11	12.0	424 (408+16)	339 [M+H-(69+16)] ⁺ , 304 [M+H-(104+16)] ⁺ , 276 [M+H-(132+16)] ⁺ , 248 [M+H-(160+16)] ⁺	C ₂₃ H ₂₂ FN ₃ O ₄	Oxidation of anlotinib	Plasma, bile, feces Plasma
M12	12.0	504 (408+16+80)	424 [M+H-80] ⁺ , 339 [M+H-80-(69+16)] ⁺ (80)	C ₂₃ H ₂₂ FN ₃ SO ₇	Sulfation of M10 or M11	Bile, urine Not detected

For dogs, only plasma samples were available.

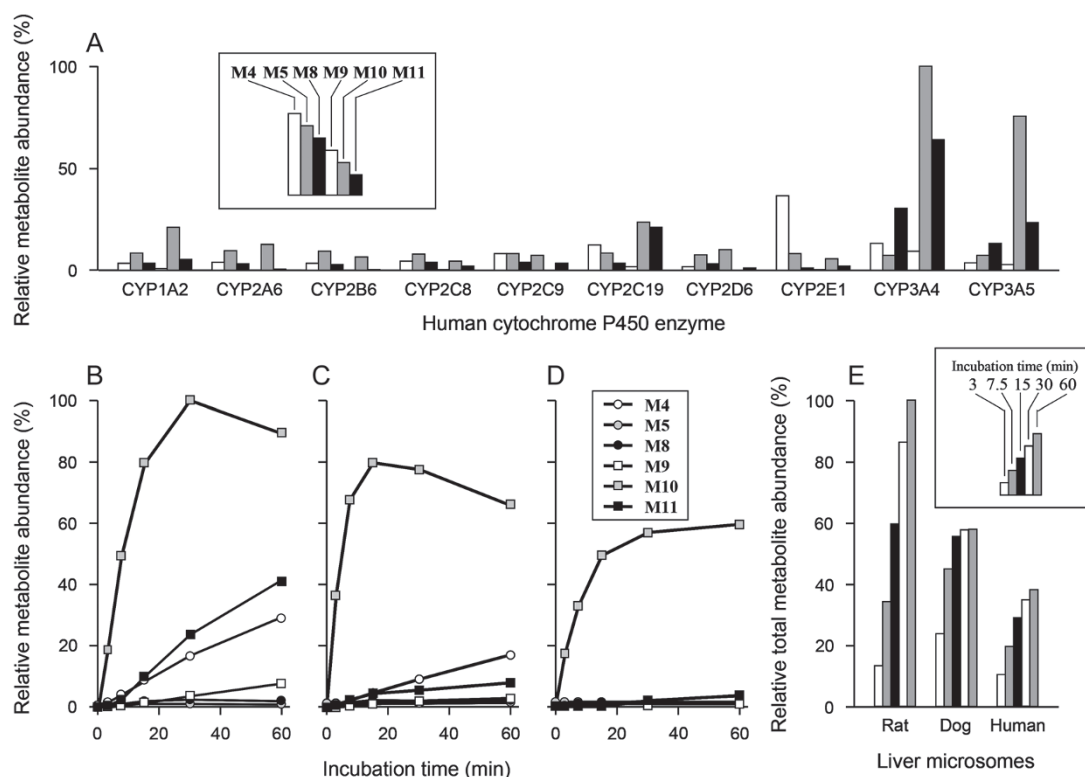


Figure 4. Human cytochrome P450 enzymes mediating *in vitro* oxidation of anlotinib (A) and comparative metabolic capabilities of liver microsomes of different species in mediating the metabolism (B–E). For the enzyme identification using cDNA-expressed human P450 enzymes, the substrate anlotinib and enzyme concentration were 2 $\mu\text{mol/L}$ and 50 pmol P450/mL, respectively, with an incubation time of 60 min. The metabolites formed were expressed as relative abundance, with the most abundant M10 being 100% after incubation with CYP3A4. For the metabolic capability comparison using rat liver microsomes (B), dog liver microsomes (C), and human liver microsomes (D), the substrate anlotinib and enzyme concentration were 2 $\mu\text{mol/L}$ and 0.5 mg protein/mL, respectively, with incubation times of 3, 7.5, 15, 30, and 60 min. The metabolites formed were expressed as relative abundance, with the most abundant M10 being 100% after incubation with rat liver microsomes for 30 min. Panel (E) shows comparative relative total abundance of M4, M5, M8, M9, M10, and M11 formed from anlotinib after incubation with NADPH-fortified rat liver microsomes, dog liver microsomes, and human liver microsomes. The chemical structures of formed metabolites were shown in Figure 3. Quantification of the oxidized metabolites was achieved using the calibration curve of anlotinib.

***In vitro* inhibitory activity of anlotinib on drug metabolism enzymes and transporters**

As shown in Table 5, anlotinib exhibited, *in vitro*, significant potency to inhibit CYP3A4 and CYP2C9 with IC_{50} values of $<1 \mu\text{mol/L}$; such inhibitory potency towards CYP2C19, CYP2C8, UGT1A1, UGT1A4, UGT1A9, and UGT2B15 was moderate, with IC_{50} values of 1–10 $\mu\text{mol/L}$. This tyrosine kinase inhibitor exhibited low inhibitory potency *in vitro* towards human CYP2B6, CYP2D6, UGT1A6, UGT2B7, OATP1B1, OAT3, OCT2, MDR1, and BCRP with values of IC_{50} greater than 10 $\mu\text{mol/L}$. No significant inhibitory potency of anlotinib was found towards human CYP1A2, CYP3A5, OATP1B3, OAT1, and MRP1. Anlotinib was not an *in vitro* substrate of OATP1B1, OATP1B3, OAT1, OAT3, OCT2, MDR1, and BCRP (Supplementary Table S1).

Discussion

Anlotinib is a new and promising tyrosine kinase inhibitor that is likely to provide an additional medication to cancer therapy. Like many approved tyrosine kinase inhibitors,

anlotinib exhibited pH-dependent hydrophilicity and lipophilicity. The compound was well soluble in acidic environment and had good membrane permeability measured at pH 7.4. Its aqueous solubility at pH 6.5 appeared to be too low to provide adequate absorption in the jejunum and the ileum. However, levels of systemic exposure to anlotinib in rats and dogs did not increase in any down-proportional manner as the oral dose increased to the highest levels. This suggested that the stomach and duodenum were probably the major absorption sites for oral anlotinib. In clinical practice, the gastrointestinal absorption of many tyrosine kinase inhibitors, including crizotinib, dasatinib, erlotinib, gefitinib, lapatinib, and pazopanib, can be substantially altered by concomitant administration of acid suppressive drugs, such as antacids, proton-pump inhibitors, and H_2 -antagonists^[17]. A similar scenario is expected to take place with (for/in) anlotinib and, if possible, coadministration of this tyrosine kinase inhibitor with acid-suppressive drugs should be avoided. Rats and dogs exhibited an interspecies difference in oral bioavailability (F) of anlotinib. Because of the passive diffusion-based

Table 5. Inhibitory effects of anlotinib on human drug metabolizing enzymes and transporters.

Enzyme or transporter	Substrate → metabolite or substrate only	Positive control inhibitor/ its concentration (μmol/L)	Percentage inhibition by positive control inhibitor (%)	Percentage inhibition by anlotinib at 100 μmol/L (%)	IC ₅₀ (μmol/L)	IC ₅₀ (ng/mL)
Human cytochrome P450s						
CYP1A2	CEC → CHC	furaflyline/100	97.0±0.0	46.7±1.0	—	—
CYP2B6	EFC → HFC	tranylcypromine/125	93.3±1.6	52.9±0.3	45.42±11.83	18487±4814
CYP2C8	DBF → fluorescein	quercetin/20	100.0±0.0	90.5±1.8	3.61±0.49	1470±199
CYP2C9	MFC → HFC	sulfaphenazole/10	94.1±2.6	98.4±1.5	0.87±0.07	357±30
CYP2C19	CEC → CHC	tranylcypromine/100	94.9±0.9	93.5±0.4	1.21±0.09	523±52
CYP2D6	AMMC → AMHC	quinidine/0.5	89.8±0.2	79.2±8.3	14.78±1.61	5919±822
CYP3A4	BFC → HFC	ketoconazole/5	97.7±0.7	96.3±0.0	0.11±0.03	43±12
CYP3A5	Midazolam → 1'-hydroxymidazolam	ketoconazole/9	85.8±0.7	33.2±0.6	—	—
Human uridine 5'-diphosphoglucuronosyltransferases						
UGT1A1	β-E2 → E3G	niflumic acid/100	93.8±8.7	92.8±1.0	3.98±0.44	1623±181
UGT1A3	4-MU → 4-MUG	atazanavir/100	85.2±1.2	43.4±8.0	—	—
UGT1A4	TFP → TFPG	hecogenin/100	90.4±0.3	79.5±3.8	6.01±1.36	2453±553
UGT1A6	4-MU → 4-MUG	phenylbutazone/100	70.1±8.0	57.4±10.9	34.25±11.91	13974±4858
UGT1A9	4-MU → 4-MUG	niflumic acid/100	99.7±0.0	85.4±1.3	2.26±0.48	923±195
UGT2B7	4-MU → 4-MUG	diclofenac/100	53.3±1.2	88.9±1.5	32.36±3.45	13206±1408
UGT2B15	SENI → SENI7G	diclofenac/100	78.6±2.4	100.0±0.0	9.94±0.86	4058±350
Human SLC transporters						
OATP1B1	E17βG	rifampin/1000	100.0±0.0	52.7±1.6	82.51±12.69	33583±5165
OATP1B3	E17βG	rifampin/1000	100.0±0.0	22.7±5.6	—	—
OAT1	para-aminohippuric acid	probenecid/1000	99.9±0.0	12.0±4.2	—	—
OAT3	estrone-3-sulfate	probenecid/1000	85.6±4.8	60.3±3.8	53.73±3.18	21869±1292
OCT2	tetraethylammonium	cimetidine/1000	93.8±1.9	70.1±0.7	26.25±5.82	10684±2369
Human ABC transporters						
MDR1	ginsenoside Rg ₁	tariquidar/1000	100.0±0.0	60.7±5.7	70.32±3.32	28691±1355
BCRP	methotrexate	novobiocin/1000	100.0±0.0	70.8±2.8	65.10±7.31	26561±2982
MRP1	E17βG	MK571/1000	97.0±4.0	11.9±1.3	—	—

CEC, 3-cyano-7-ethoxycoumarin; CHC, 3-cyano-7-hydroxycoumarin; EFC, 7-ethoxy-4-trifluoromethylcoumarin; HFC, 7-hydroxytrifluoromethylcoumarin; DBF, dibenzylfluorescein; MFC, 7-methoxy-4-trifluoromethylcoumarin; AMMC, 3-[2-(N,N-diethyl-N-methylamino)ethyl]-7-methoxy-4-methylcoumarin; AMHC, 3-[2-(N,N-diethylamino)ethyl]-7-hydroxy-4-methylcoumarin; BFC, 7-benzyloxy-trifluoromethylcoumarin; β-E2, β-estradiol; E3G, β-estradiol-3-β-D-glucuronide; 4-MU, 4-methylumbelliferon; 4-MUG, 4-methylumbelliferyl-β-D-glucuronide; TFP, trifluoperazine; TFPG, trifluoperazine-N-β-D-glucuronide; SENI, senkyunolide I; SENI7G, senkyunolide I-7-O-β-glucuronide; and E17βG, estradiol-17β-D-glucuronide.

intestinal absorption (suggested by the Caco-2 data), the extensive hepatic uptake but limited hepatobiliary excretion (suggested by the rat data in Table 1), and the interspecies difference in extent of P450-mediated oxidation (suggested by the *in vitro* metabolism data in Figure 4), the *F* difference probably resulted mainly from the interspecies difference in the first-pass enterohepatic metabolic clearance. Absolute *F* of anlotinib has not been assessed in cancer patients^[3], because intravenous anlotinib was not available for the human study. Based on the interspecies differences in the *in vitro* metabolism (Figure 4), the human oral bioavailability of anlotinib was estimated at 41%–77%, which was higher than, or at least as high as, the dog oral bioavailability.

Consistent with its rapid intestinal absorption, anlotinib exhibited comparable values of terminal half-lives ($t_{1/2}$), after intravenous and oral administration, in rats and dogs, suggesting that the $t_{1/2}$ for oral administration reflected the compound's elimination rate during the terminal phase, rather

than the absorption rate. In other words, flip-flop pharmacokinetics did not exist for orally administered anlotinib in rats and dogs. The $t_{1/2}$ of anlotinib was significantly longer in dogs than in rats. Anlotinib exhibited, in both rats and dogs, large values of V_{SS} , which were 40 and 12 times as much as the volumes of total body water of rat and dog, respectively^[15]. Therefore, the preceding $t_{1/2}$ difference between rats and dogs was mainly attributed to the interspecies difference in $CL_{tot,p}$ (Table 1). *In vivo* and *in vitro* pharmacokinetics and metabolism data suggested that cytochrome P450-mediated oxidation was the major elimination pathway of anlotinib and controlled the $CL_{tot,p}$. Consistent with comparative metabolic capabilities of hepatic P450 mediating its oxidation: rat>dog>human, anlotinib exhibited, in patient volunteers with advanced refractory solid tumors, a very long $t_{1/2}$ (96±17 h)^[3], which was also related to a large V_{SS} and a slow $CL_{tot,p}$. Anlotinib has a significantly longer $t_{1/2}$ in cancer patients than most tyrosine kinase inhibitors approved to date (3–60 h)^[18]. Based on this

pharmacokinetic characteristic, a “two-week on/one-week off” dosage regimen was designed to achieve efficacy and safety in anlotinib-based cancer therapy^[3].

In rats and in tumor-bearing mice, total (unbound plus bound) concentrations of anlotinib in various tissues, including the tumor tissue, were significantly higher than the associated total (unbound plus bound) plasma concentrations. The higher total levels of tissue exposure to anlotinib were in agreement with large apparent volumes of distribution in the animals; this resulted from binding competition between the tissues and the plasma. Such binding competition is expected to take place in humans as well. The high total levels of tissue exposure do not imply high intracellular concentrations of unbound anlotinib in the tissues. The therapeutic intracellular unbound concentration of anlotinib in the tumor tissue is equal to the unbound plasma concentration under the distribution equilibrium condition. Accordingly, a change in unbound concentration of anlotinib in plasma has a large effect on its intracellular unbound concentration. Anlotinib was highly bound in human plasma with a f_u of 7%; this binding was predominantly to albumin and lipoproteins, with other plasma proteins playing only a minor role. Affinity of anlotinib for lipoproteins, particularly for low density lipoproteins and very low density lipoproteins, was substantially higher than its affinity for albumin and α_1 -acid glycoprotein. While anlotinib exhibited affinity for α_1 -acid glycoprotein comparable to that of imatinib (Gleevec), influence of α_1 -acid glycoprotein on pharmacokinetics of anlotinib is probably limited. Unlike anlotinib, imatinib exhibited affinity for α_1 -acid glycoprotein substantially higher than its affinity for albumin, with an nK ratio of 92. Such an nK ratio for anlotinib was 1. The plasma protein α_1 -acid glycoprotein is mainly synthesized and metabolized in the liver and also expressed in malignant cells and its level may be elevated significantly in patients with malignant tumors^[7,19]. Varying level of α_1 -acid glycoprotein could interfere with measurement of the plasma concentration of imatinib, rendering such concentration unreliable as surrogate marker of tumor intracellular concentration^[20,21]. Although many approved tyrosine kinase inhibitors, such as axitinib (Inlyta), lapatinib (Tykerb), and vemurafenib (Zelboraf) ($f_{ur} < 1\%$), are highly bound in human plasma, little evidence is available to support their interactions with other highly bound drugs^[17]. This is probably because proteins other than albumin and α_1 -acid glycoprotein also significantly contribute to binding of these tyrosine kinase inhibitors in plasma. Like anlotinib, imatinib was found to have high affinity for lipoproteins, which contribute significantly to its binding in plasma (Table 3). Lipoproteins might also significantly contribute to binding of other tyrosine kinase inhibitors, also basic molecules, in plasma.

Multiple human P450 isoforms could mediate anlotinib's oxidative metabolism that governed its clearance from the systemic circulation, albeit CYP3A4 and CYP3A5 exhibiting the greatest *in vitro* metabolic capabilities. This suggests that significant alteration of the anlotinib metabolism in the liver via enzyme inhibition by coadministered drug(s) requires

affecting the concerted action of multiple P450 enzymes, rather than affecting the function of a single enzyme. In other words, circulating anlotinib has a low propensity to be a victim of hepatic drug interactions by inhibiting the P450 enzymes. Given that the positioning of the intestine as the first site of exposure of xenobiotics to the body's metabolic system and that CYP3A represents the largest piece (82%) of the intestinal P450 pie^[22,23], inhibition of intestinal CYP3A during absorption probably results in increased systemic exposure to anlotinib. In addition, induction of the P450 enzymes, particularly CYP3A and CYP2C, may result in decreased systemic exposure to anlotinib. Meanwhile, anlotinib was found to be a potent *in vitro* inhibitor of CYP3A4 (IC_{50} 0.1 $\mu\text{mol/L}$) and CYP2C9 (0.9 $\mu\text{mol/L}$). Based on its multiple-dose human plasma pharmacokinetics^[3], drug interaction indices, as calculated by unbound plasma C_{max}/IC_{50} , were 0.16 for CYP3A4 and 0.02 for CYP2C9, suggesting that circulating anlotinib also had a low propensity to precipitate drug interactions on these P450 isoforms. CYP3A4 and CYP3A5 have similar substrate specificity and exhibit high (84%) amino acid sequence identity^[24,25]. Despite being the substrate of CYP3A4 and CYP3A5 with comparable *in vitro* metabolic capabilities, anlotinib exhibited very much different inhibitory potency against these P450 isoforms (IC_{50} >100 $\mu\text{mol/L}$ for CYP3A5). These data also suggested that inhibition of CYP3A4 by anlotinib had limited influence on pharmacokinetics of this tyrosine kinase inhibitor.

The majority of approved tyrosine kinase inhibitors are reported to cause hepatotoxicity that requires careful patient management to maintain treatment benefit without harm^[26,27]. Some tyrosine kinase inhibitors, such as erlotinib (Tarceva) and sorafenib (Nexavar), have been observed to cause hyperbilirubinemia^[28,29]. Since UGT1A1-mediated hepatic glucuronidation plays a key role in clearance of bilirubin from the systemic circulation, deficiency of this enzyme results in elevated serum level of total bilirubin^[30,31]. Due to growing recognition of the importance of drug-bilirubin interactions, many tyrosine kinase inhibitors were assessed with respect to their inhibition of UGT1A1 activity^[32-36]. Anlotinib inhibited UGT1A1-mediated β -estradiol glucuronidation, a surrogate for UGT1A1-mediated bilirubin glucuronidation, with an IC_{50} of 4.0 $\mu\text{mol/L}$; the UGT1A1 inhibition by anlotinib appeared less potent than those by erlotinib (IC_{50} 0.7 $\mu\text{mol/L}$, against *N*-3-carboxy propyl-4-hydroxy-1,8-naphthalimide glucuronidation)^[36] and sorafenib (0.1 $\mu\text{mol/L}$, against 4-methylumbelliferone glucuronidation)^[35]. In addition, unbound C_{max} values of anlotinib, erlotinib, and sorafenib at their respective clinically relevant doses were 0.02, 0.21, and 0.06 $\mu\text{mol/L}$, respectively^[3,17,26]. Although the extent of UGT1A1 inhibition that is required to precipitate hyperbilirubinemia is unclear, anlotinib is believed to have a lower propensity to cause hyperbilirubinemia than erlotinib and sorafenib. In the phase I clinical trial to evaluate safety, pharmacokinetics, and efficacy of anlotinib, only mild total bilirubin elevation was reported in 33% (Grade 1) and 5% (Grade 2), of patients with advanced refractory solid tumors, while no incidence of severe hyperbilirubinemia (Grades 3-5) was reported^[3].

Development of multidrug resistance is a leading cause of cancer treatment failure; the molecular basis of such resistance involves transporter-mediated drug efflux, kinase domain mutations, DNA damage repair, activation of alternative signaling pathways, and evasion of cell death^[37]. Increasing data suggest that MDR1 and BCRP are two transporters significantly contributing to resistance to tyrosine kinase inhibitors^[38]. Combination drug therapy has been suggested to offer advantages for treatment of drug-resistant cancers. Although inhibitors of MDR1 and BCRP can be explored to overcome resistance to tyrosine kinase inhibitors that are substrates of these transporters in tumors, such drug combinations might enhance toxicity of these tyrosine kinase inhibitors by elevating their concentrations in normal tissues that express the transporters. Similarly, combinations of tyrosine kinase inhibitor that potently inhibit the transporter activity with cytotoxic anticancer drugs that are the transporter substrates might also yield desired pharmacokinetic drug interactions in tumor tissues but undesired ones in the normal tissues as well. Accordingly, the ideal tyrosine kinase inhibitor should not be a substrate or modulator of the ABC transporters^[38]. Anlotinib was found not to be a substrate of MDR1 and BCRP, suggesting that it has a low propensity to develop intrinsic or acquired resistance arising from drug efflux from tumor cells. Meanwhile, anlotinib was not a potent inhibitor of these transporters as well, suggesting that coadministered drugs in anlotinib-including combinations are more likely to exert synergistic or additive pharmacodynamic effect as well as exhibit pharmacokinetic compatibility (*ie*, without any pharmacokinetic drug interactions) in the treatment of drug-resistant cancers.

Anlotinib exhibits multiple pharmacokinetic characteristics similar to those of many approved tyrosine kinase inhibitors, including good gastrointestinal absorption with pH-dependent water solubility and membrane permeability, high binding in plasma, and large apparent volume of distribution. Also, P450-mediated oxidation is a key factor governing anlotinib's oral bioavailability, clearance from the systemic circulation, terminal half-life, and associated interspecies differences. Compared with many approved tyrosine kinase inhibitors, anlotinib appears to have a low propensity to precipitate drug interactions via inhibition of many major drug metabolizing enzymes and transporters at its clinically relevant dose. Acid-suppressive drugs and intestinal CYP3A4 modulating drugs may interact with anlotinib. Anlotinib has a low propensity to cause hyperbilirubinemia and to develop resistance arising from transporter-mediated efflux from tumor cells. In human plasma, anlotinib is predominantly bound to albumin and lipoproteins; influences of varying levels of albumin and lipoproteins on pharmacokinetics of anlotinib and on its tumor intracellular concentration remain to be investigated in cancer patients.

Author contribution

Chuan LI, Feng CHEN and Wei NIU designed the research; Feng CHEN, Wei NIU, Chen-chun ZHONG, Jun-ling YANG, Wei-wei JIA, Li LI, Chen CHENG, Fei-fei DU, Su-ping

ZHANG, Cheng-ying XIE, Na-ting ZHANG, Olajide E OLAL-EYE, Feng-qing WANG, Fang XU, Li-guang LOU, and Dong-ying CHEN performed the research; Chuan LI, Wei NIU, Chen-chun ZHONG, and Feng CHEN analyzed data; and Chuan LI and Wei NIU wrote the paper.

Supplementary information

Supplementary information is available on the website of *Acta Pharmacologica Sinica*.

References

- 1 Krause DS, Van Etten RA. Tyrosine kinases as targets for cancer therapy. *N Engl J Med* 2005; 353: 172–87.
- 2 Arora A, Scholar EM. Role of tyrosine kinase inhibitors in cancer therapy. *J Pharmacol Exp Ther* 2005; 315: 971–9.
- 3 Sun YK, Niu W, Du F, Du CX, Li ST, Wang JW, et al. Safety, pharmacokinetics, and antitumor properties of anlotinib, an oral multi-target tyrosine kinase inhibitor, in patients with advanced refractory solid tumors. *J Hematol Oncol* 2016; 9: 105.
- 4 Han BH. Efficiency and safety of anlotinib hydrochloride as 3rd line treatment or beyond in patients with advanced NSCLC in ALTER-003 study, a randomized, double-blind, placebo-controlled Phase III trial in China. The American Society of Clinical Oncology Annual Meeting, Chicago, IL, USA, June 2–6, 2017, Abstract 182187.
- 5 Guo B, Li C, Wang GJ, Chen LS. Rapid and direct measurement of free concentrations of highly protein-bound fluoxetine and its metabolite norfluoxetine in plasma. *Rapid Commun Mass Spectrom* 2006; 20: 39–47.
- 6 Li J, Brahmer J, Messersmith W, Hidalgo M, Baker SD. Binding of gefitinib, an inhibitor of epidermal growth factor receptor-tyrosine kinase, to plasma proteins and blood cells: *in vitro* and in cancer patients. *Invest New Drugs* 2006; 24: 291–7.
- 7 Zsila F, Fitos I, Bencze G, Kéri G, Órfi L. Determination of human serum α_1 -acid glycoprotein and albumin binding of various marketed and preclinical kinase inhibitors. *Curr Med Chem* 2009; 16: 1964–77.
- 8 Dai JY, Yang JL, Li C. Transport and metabolism of flavonoids from Chinese herbal remedy Xiaochaihu-tang across human intestinal Caco-2 cell monolayers. *Acta Pharmacol Sin* 2008; 29: 1086–93.
- 9 Li L, Zhao YS, Du FF, Yang JL, Xu F, Niu W, et al. Intestinal absorption and presystemic elimination of various chemical constituents present in GBE50 extract, a standardized extract of *Ginkgo biloba* leaves. *Curr Drug Metab* 2012; 13: 494–509.
- 10 Kerns EH, Di L. Drug-like properties: concepts, structure design and methods: from ADME to toxicity optimization. 1st ed. Burlington: Academic Press; 2008. p 283 (equilibrium shake flask thermodynamic solubility method), p 267–8 (shake flask method for lipophilicity).
- 11 Hu ZY, Yang JL, Cheng C, Huang YH, Du FF, Wang FQ, et al. Combinatorial metabolism notably affects human systemic exposure to ginsenosides from orally administered extract of *Panax notoginseng* roots (Sanqi). *Drug Metab Dispos* 2013; 41: 1457–69.
- 12 Jiang RR, Dong JJ, Li XX, Du FF, Jia WW, Xu F, et al. Molecular mechanisms governing different pharmacokinetics of ginsenosides and potential for ginsenoside-perpetrated herb-drug interactions on OATP1B3. *Br J Pharmacol* 2015; 172: 1059–73.
- 13 Jia WW, Du FF, Liu XW, Jiang RR, Xu F, Yang JL, et al. Renal tubular secretion of tanshinol: molecular mechanisms, impact on its systemic exposure, and propensity for dose-related nephrotoxicity and for renal herb-drug interactions. *Drug Metab Dispos* 2015; 43: 669–78.
- 14 Smith BP, Vandenhende FR, DeSante KA, Farid NA, Welch PA,

- Callaghan JT, *et al*. Confidence interval criteria for assessment of dose proportionality. *Pharm Res* 2000; 17: 1278–83.
- 15 Davies B, Morris T. Physiological parameters in laboratory animals and humans. *Pharm Res* 1993; 10: 1093–5.
- 16 Lipinski CA. Drug-like properties and the causes of poor solubility and poor permeability. *J Pharmacol Toxicol Methods* 2000; 44: 235–49.
- 17 van Leeuwen RWF, van Gelder T, Mathijssen RHJ, Ajansman FG. Drug-drug interactions with tyrosine-kinase inhibitors: a clinical perspective. *Lancet Oncol* 2014; 15: e315–26.
- 18 van Erp NP, Gelderblom H, Guchelaar HJ. Clinical pharmacokinetics of tyrosine kinase inhibitors. *Cancer Treat Rev* 2009; 35: 692–706.
- 19 Lee SY, Lim JW, Kim YM. Effect of alpha-1-acid glycoprotein expressed in cancer cells on malignant characteristics. *Mol Cell* 2001; 11: 341–5.
- 20 Widmer N, Decosterd LA, Csajka C, Leyvraz S, Duchosal MA, Rosselet A, *et al*. Population pharmacokinetics of imatinib and the role of α_1 -acid glycoprotein. *Br J Clin Pharmacol* 2006; 62: 97–112.
- 21 Apperley JF. Part I: mechanisms of resistance to imatinib in chronic myeloid leukaemia. *Lancet Oncol* 2007; 8: 1018–29.
- 22 Kaminsky LS, Zhang QY. The small intestine as a xenobiotic-metabolizing organ. *Drug Metab Dispos* 2003; 31: 1520–5.
- 23 Paine MF, Hart HL, Ludington SS, Haining RL, Rettie AE, Zeldin DC. The human intestinal cytochrome P450 “PIE”. *Drug Metab Dispos* 2006; 34: 880–6.
- 24 Thummel KE, Wilkinson GR. *In vitro* and *in vivo* drug interactions involving human CYP3A. *Annu Rev Pharmacol Toxicol* 1998; 38: 389–430.
- 25 Aoyama T, Yamano S, Waxman DJ, Lapenson DP, Meyer UA, Fischer Vpperley, *et al*. Cytochrome P-450 hPCN3, a novel cytochrome P-450 IIIA gene product that is differentially expressed in adult human liver. cDNA and deduced amino acid sequence and distinct specificities of cDNA-expressed hPCN1 and hPCN3 for the metabolism of steroid hormones and cyclosporine. *J Biol Chem* 1989; 264: 10388–95.
- 26 Shah RR, Morganroth J, Shah DR. Hepatotoxicity of tyrosine kinase inhibitors: clinical and regulatory perspectives. *Drug Saf* 2013; 36: 491–503.
- 27 Spraggs CF, Xu CF, Hunt CM. Genetic characterization to improve interpretation and clinical management of hepatotoxicity caused by tyrosine kinase inhibitors. *Pharmacogenomics* 2013; 14: 541–54.
- 28 Jakacki RI, Hamilton M, Gilbertson RJ, Blaney SM, Tesak J, Krailo MD, *et al*. Pediatric phase I and pharmacokinetic study of erlotinib followed by the combination of erlotinib and temozolomide: a children’s oncology group phase I consortium study. *J Clin Oncol* 2008; 26: 4921–7.
- 29 Abou-Alfa GK, Amadori D, Santoro A, Figer A, De Greve J, Lathia C, *et al*. Safety and efficacy of sorafenib in patients with hepatocellular carcinoma (HCC) and Child-Pugh A versus B cirrhosis. *Gastrointest Cancer Res* 2011; 4: 40–4.
- 30 Bosma PJ, Goldhoorn B, Bakker C, Oude Elferink RP, Chowdhury JR, Chowdhury NR, *et al*. Bilirubin UDP-glucuronosyltransferase 1 is the only relevant bilirubin glucuronidating isoform in man. *J Biol Chem* 1994; 269: 17960–4.
- 31 Tukey RH, Strassburg CP. Human UDP-glucuronosyltransferases: metabolism, expression, and disease. *Annu Rev Pharmacol Toxicol* 2000; 40: 581–616.
- 32 Liu Y, Ramirez J, House L, Ratain M. Comparison of the drug-drug interactions potential of erlotinib and gefitinib via inhibition of UDP-glucuronosyltransferases. *Drug Metab Dispos* 2010; 38: 32–9.
- 33 Ai L, Zhu LL, Yang L, GE GB, Cao YF, Liu Y, *et al*. Selectivity for inhibition of nilotinib on the catalytic activity of human UDP-glucuronosyltransferases. *Xenobiotica* 2014; 44: 320–5.
- 34 Zhang N, Liu Y, Jeong H. Drug-drug interaction potentials of tyrosine kinase inhibitors via inhibition of UDP-glucuronosyltransferases. *Sci Rep* 2015 ; 5: 17778.
- 35 Miners JO, Chau N, Rowland A, Burns K, McKinnon RA, Mackenzie PI, *et al*. Inhibition of human UDP-glucuronosyltransferase enzymes by lapatinib, pazopanib, regorafenib and sorafenib: implications for hyperbilirubinemia. *Biochem Pharmacol* 2017; 129: 85–95.
- 36 Cheng XW, Lv X, Qu HY, Li DD, Hu MM, Guo WZ, *et al*. Comparison of the inhibition potentials of icotinib and erlotinib against human UDP-glucuronosyltransferase 1A1. *Acta Pharm Sin B* 2017; 7: 657–64.
- 37 Holohan C, Schaeysbroeck SV, Longley DB, Johnston PG. Cancer drug resistance: an evolving paradigm. *Nat Rev Cancer* 2013; 13: 714–26.
- 38 Shukla S, Chen ZS, Ambudkar SV. Tyrosine kinase inhibitors as modulators of ABC transporter-mediated drug resistance. *Drug Resist Update* 2012; 15: 70–80.